Construction and Building Materials 151 (2017) 809–818

Contents lists available at ScienceDirect

Construction and Building Materials

journal homepage: www.elsevier.com/locate/conbuildmat

Electrokinetic and thermodynamic characterization of lime-water interface: Physical and rheological properties of lime mortar

E. Ontiveros-Ortega [a], A. Ontiveros-Ortega [b,c,*], J.A. Moleon [b], E. Ruiz-Agudo [d]

[a] Andalusian Historical Heritage Institute (AHHI), Geology Laboratory (Spain), Avda. de Los Descubrimientos S/N, 41092 Sevilla, Spain
[b] Department of Physics, University of Jaén (Spain), Campus Universitario de las Lagunillas s/n, edificio A-3, 23071 Jaén, Spain
[c] Instituto Andaluz de Geofísica, University of Granada, Fuentenueva s/n, 18002 Granada, Spain
[d] Department of Mineralogy and Petrology l, University of Granada, 18071 Granada, Spain

HIGHLIGHTS

- The calcination process of limestone modifies the surface free energy of the lime.
- Quicklime is more hydrophilic when produced in a traditional kiln between 850–900 °C.
- ξ potential of traditional quicklime were much larger than industrial quicklime.
- The traditional process generates products with more plasticity.

ARTICLE INFO

Article history:
Received 3 October 2016
Received in revised form 20 June 2017
Accepted 22 June 2017

Keywords:
Lime
Quicklime
Portlandite
Putty lime
ξ potential
Surface free energy

ABSTRACT

The surface properties of the portlandite are very important in the behavior of the suspensions of lime used as binders, plasters, mortars and paint, for use in the architecture heritage conservation. These rheological properties depend heavily on surface thermodynamic properties, surface tension-surface free energy and load the lime present in aqueous medium. It selected two types of quicklime, originating from the same rock but made in two types of kilns: traditional and industrial Kiln. It has determined values of the surface free energy of the lime in the form of CaO and $Ca(OH)_2$ as well as the rock used in its preparation. In addition, it conducted an electrokinetic study to determine electrophoretic mobility in a water/lime system. It analyzed various types of oxides after laboratory slaking and periods during which the portlandite remained in water. This study revealed that quicklime is monopolar and has a hydrophilic nature. Tradition quicklime, γ^{Total} values decrease as temperature increases the calcination of limestone. This has greater hydrophilicity than that of industrial quicklime. Moreover, traditional lime, introduces more charges than that fabricated by industrial processes, with larger values of ξ Potential. ξ Potential data confirm the optimal plasticity properties of the traditional lime, and that this quality is maintained.

1. Introduction

Lime has been used since ancient times as a material to improve cohesion used in construction materials [1]. The recoveries of traditional construction activities currently constitute an area of interest for product design, regarding its application in restoration [2]. Traditional and semi-industrialized products based on lime constitute a proposal that has been growing in recent years.

Lime is a binder obtained through a group of processes that are encompassed within the term *lime cycle*. This cycle includes a first stage of calcination of limestone between 850 and 900 °C to obtain quicklime (CaO). The dissociation temperature of $CaCO_3$ occurs at 898 °C when pCO_2 is 1 atm. This temperature is reduced by decreasing the pCO_2, and increases with its increase [3]. The end result is collapse of the crystal structure of $CaCO_3$ [4].

In the calcination process, the type of kiln, burning time, size of carbonate particles, density, and limestone purity are important in their properties [5–8]. Quicklime from traditional manufacturing (longer calcination and variable temperature inside kiln) has a slow hydration and lower slaking temperature (850–900 °C) than the industrial quicklime process (faster calcination in the kiln) [9] Lime formed during a relatively short period of calcination has a more porous structure and is highly reactive [3]. It appears

* Corresponding author at: Department of Physics. University of Jaén (Spain), Campus Universitario de las Lagunillas s/n, edificio A-3 dep.414, 23071 Jaén, Spain.
E-mail address: aontiver@ujaen.es (A. Ontiveros-Ortega).

http://dx.doi.org/10.1016/j.conbuildmat.2017.06.147
0950-0618/

that the thermal decomposition and chemical reaction control the process, influenced by the speed of calcination [10].

The process of slaking has been extensively studied in recent years [3,11–17]. The type of slaking has a significant impact on the resulting product. A supply of excess water during hydration favors the dispersion of particles, reducing their tendency to agglomerate [18]. The primary and aggregated crystals generated during and just after slaking, control the evolution of the portlandite microstructure [11,18], and improve its rheological properties while it remains in suspension in water. These crystals constitute the largest particle size because of agglomeration orientation, characteristics that most strongly affect the loss of plasticity [2,17].

The zeta (ξ) potential is one of the fundamental parameters controlling the interaction of the particles in suspension. Colloidal particles dispersed in a solution are electrically charged because of their ionic characteristics and bipolarity. According to extended DLVO (Derjaguin-Landau-Verwey-Overbeek) theory [19,20] three types of interfacial interactions should be considered, i.e., Lifshitz-van der Waals (LW), electrostatic (EL), and acid-base (AB). Their contributions depend on the nature of the interfaces involved (i.e., the ξ potential and surface free energy components).

The rheological behavior of putty lime depends on the aggregation or dispersion of portlandite nanoparticles in aqueous suspension [11] and is a function of many factors that can be classified into four groups. These are the distribution and sizes of particles, the shape and surface area of the particles, concentration and ξ potential of the dispersion [11,12,21,22].

In the present paper, the properties of surface free energy and ξ potential are determined. The objective is to understand how they affect production technology in the surface properties of the lime and the effect on them the time that this material remains in water (aging of lime putty). In terms of these parameters, it can explain better the properties of slaking lime and its rheological behavior. These properties are of interest in the advancement of knowledge of this high-value construction material.

It used for this study lime from the *Moron de la Frontera* City (Seville, Spain), which currently has two forms of quicklime production, traditional and industrial. This unique case allows greater control of variables involved in the production process such as the nature of the limestone, as reflected in previous works [6], kiln type and its technological implications; such as the effect of calcination temperature and heating rate [3,8,18,23,24].

The exceptional production conditions of such lime has made it an object of study for application in restoration works of Cultural Heritage [11,12,25–27] demonstrating its quality as a building material. In November 2011, declared Intangible Heritage of Humanity, in the category of Best Practices by UNESCO [28].

2. Material and experimental methods

2.1. Production process lime and limestone source

Traditional Kilns lime of the arabic type, to produce lime (Fig. 1) fed by combustible vegetation of olive and pine. These kilns operate with a volume of stone around 70 tons; with calcination times from 10 to 20 days (depending on environmental conditions and kiln size), with continuous feed every 15 min and a substantial daily consumption of wood. Temperatures reached inside the kiln vary from 1100 °C, at the heat source, to 750 °C, in outer areas. Smoke color, from black to white, and change in color of the stone, from reddish orange to yellow-gold observed in the upper recesses of the kiln (*caños o troneras*), facilitate the determination of the exact burning of the stone [28].

The kiln assembly is critical to the quality of the lime produced, because it is designed so that the temperature to which the stone is subjected in its interior is as homogeneous as possible. The assembly of vaults of the kiln and its structure (*Ahornado* process) is done via the method of *dry stone*, built with *armaderas* (larger stones) in a concentric arrangement. These stones are fit with other smaller stones called *matacanes* and, finally, the gaps are filled with other small stones called *ripios* [29]. This design allows that temperature inside the kiln to be as homogeneous as possible. Slaking lime is done by *spraying* (powder Lime) and traditional procedure by *fusion* (putty lime) with mechanical agitation in large amounts of oxide over 30 days. This initiates a slow increase in temperature, not exceeding 100 °C.

Fig. 1. Traditional lime kiln, Morón de la Frontera, Seville (Spain).

In industrial lime production used discontinuous vertical kilns fed with combustible natural gas, coke, fuel and oil. Limestone is subjected to temperatures between 900 and 1000 °C, over short periods of time, obtaining quicklime that is then sieved, crushed or ground and finally hydrated to obtain a very fine dry powder (powder lime).

Limestone used from the geological *Unit of the Sierra de Estepa* (External Areas of the Baetic Chain, Spain). They are constituted by micritic, oncolitic and oolitic limestone of age lower and mid-Jurassic [30].

The limestones, although having textural variations, have high purity (>90% CaO with <1% SiO_2) and very similar levels of major and trace elements. Generally, these correspond to very compact limestone with porosities 5–10%. From the standpoint of pore size distribution, two types can be distinguished. These are a variety with micropore sizes largely <2 mm and a more porous type with the presence of micropores and macropores [31].

3. Samples

It carried out a comparative study of three types of quicklime (CaO) (see Table 1). Two of these were obtained from the same limestone, but with different manufacturing technologies. These were traditional continuous vertical kilns (***TL***) (Fig. 2a), industrial continuous vertical kilns (***IL***) (Fig. 2b), and commercial lime, supplied by Panréac with analytical purity (ref: 211234.1211; lot: 0000534420 M = 56.08 g/mol; ***PL***).

Traditional Kilns are characterized by heterogeneous burning. Thus, for the *TL* lime it analyzed three varieties, located in different areas of the kiln with different calcination temperatures. These were TL (1) (1100 °C), TL (2) (900 °C) and TL (3) (850 °C). This was done to see if temperature changes affected the surface free energy properties and ξ potential of lime.

In the laboratory, it prepared lime putty from the quicklime (CaO) obtained by two calcination processes, traditional (SPL_{TL}) and industrial (SPL_{IL}). The slaking was done in distilled water in a lime/water ratio of 1:3, without stirring. The hydrates were also made from quicklime of analytical purity (SPL_{PL}).

Table 1
CaO Samples and corresponding $Ca(OH)_2$ obtained of hydrations at 0 and 6 months.

Samples	Burning temperatures	Corresponding Ca $(OH)_2$ (O-6 month)
TL(CaO) Traditional method. Francisco Gordillo's lime	**TL(1)** 1100 °C	**SPL_{TL}(1)**
	TL(2) 900 °C	**SPL_{TL}(2)**
	TL(3) 850 °C	**SPL_{TL}(3)**
IL(CaO) Industrial method. Calcinor, Andalusian of Limes	1000 °C	**SPL_{IL}**
PL(CaO) Analytical purity. PANREAC AppliChem	¿?	**SPL_{PL}**

Fig. 2. a) Quicklime (*TL*) obtained by traditional process. b) Quicklime (*IL*) obtained by industrial process. c) limestone from Gilena quarry d) limestone from Morón de la Frontera quarry.

Ancient manuals construction and the scientific literature indicate that hydrated lime improves its plasticity properties with time [18]. It determined the ξ potential of the putty lime at two times, t = 0 (recently slaked) and t = 6 months, to see if time affected the electrophoretic mobility of the portlandite particles.

On the other hand, it analyzed limestone used in the production of lime, specifically, two varieties extracted from quarries of the village of *Gilena* (see Fig. 2c) and *Moron de la Frontera* (see Fig. 2d) (both near Seville). The latter had historical exploitation but is currently inactive. It has been declared a Heritage of Cultural Interest by the Junta of Andalusia (Spain) and was traditionally used for lime production (see Table 2).

4. Methods

4.1. Compositional analysis of the samples

The mineralogical composition of the materials was evaluated by X-ray diffraction (XRD), using a D8 DISCOVER diffractometer with Cu-Ka radiation. The XRD patterns were collected using Co kα1 (λkα1 = 1.7889 Å) and kα2 (λkα2 = 1.7928 Å) radiation in the range Δ2θ = 3–70° with a step size of 0.015° and a counting time of 0.1 s per step. The chemical composition of major and trace elements was done using the Phillips X-ray Fluorescence (XRF) mini-trace method and PANalytical AXIOS Rh spectrometer. A scanning electron microscope FESEM (FEI-TENEO), acceleration voltage: 200 eV–30 keV (20 eV with BD), was used to analyze microstructure, particle morphology and texture relationships. Thin sections of quarry samples were examined with a Leica DMLP petrographic polarizing microscope and a camera with a Leica DFC 280 digital image capture system. The particle size distribution (PSD), range between 0.02 and 2000 μm, of slaking lime (putty lime) dispersions was measured using a Coulter LS 230 laser diffraction particle size analyser.

Table 2
Limestone samples.

Quarry samples	Description
Q1	Historic quarry from Morón de la Frontera, Seville. Spain
Q2	Gilena quarry A, Seville
Q3	Gilena quarry B, Seville

4.2. Surface free energy determination

For determination of the surface free energy of the material, two techniques were used. First, the contact angle on thermodynamically stable surfaces was obtained by a pressing, or by a liquid penetration thin-layer technique (layer wicking) if we were unable to achieve stable surfaces.

To estimate the surface free energy of the different types of limes, it used measurement of increasing contact angles of three probe liquids (diiodomethane, water, and formamide) of known surface-tension components, on dry pellets a centimeter in diameter. For this purpose, a ramé–Hart Inc. (USA) NRL CA goniometer was used. The image of drops placed on the surface was captured by a video camera adapted to the goniometer, immediately after their deposition with a Gilmont (USA) micrometer syringe.

Prior to contact angle measurements, the pellets were dried at 70 °C and kept in a desiccator. Only stable drops were used to compute the surface free energy components of the solids. The contact angle of the same set of liquids was similarly measured on quicklime, slaking lime, putty lime and stone pellets made by compressing dry powder under 1.5×10^4 kg/cm^2 pressure for 10 min.

Only pellets with a smooth, specular surface (at the optical microscope level) were selected. Detailed descriptions of the [19] approach to surface free energy formulation were given in numerous papers from those authors [19,20]. Thus, the total surface free energy of a solid or a liquid is described as the sum of the LW component γ_S^{LW} (including London dispersion—the main interaction—Debye polarization, and Keeson orientation) and AB interaction γ_S^{AB}, in many cases due to hydrogen bonding. In general, the polar γ^{AB} interaction is due to the electron-donor, γ^-, and electron-acceptor, γ^+, contributions. The relationship between contact angle θ and the LW and (Lewis) AB components of the surface free energy of the

Table 3
Surface free energy components (mJ/m^2) of liquids used in contact angle measurements.

Liquid	γ^{TOTAL}	γ^{LW}	γ^+	γ^-
Water	72.8	21.8	25.5	25.5
Formamide	58.0	39.0	39.6	2.28
Diiodomethane	50.8	50.8	0.0	0.0

solid (subscript 1) and surface tension of the liquid (subscript 3) can be written as

$$2\sqrt{\gamma_1^{LW}\gamma_{Li}^{LW}} + 2\sqrt{\gamma_1^{+}\gamma_{Li}^{-}} + 2\sqrt{\gamma_1^{-}\gamma_{Li}^{+}} = \gamma_{Li}(1+\cos\theta), \quad (1)$$

where γ_{Li} is the surface tension of liquid *i* forming contact angle θ on the solid, and γ_{Li}^{LW}, γ_{Li}^{+}, and γ_{Li}^{-} are the surface tension components of the liquid.

Thus, by measuring the θ of the three liquids mentioned, a system of three equations of type (1) can be resolved to attain the three unknown variables γ_1^{LW}, γ_1^{+}, and γ_1^{-}. The surface free energy components of the liquids used are shown in Table 3.

4.3. Electrophoretic mobility

To estimate the surface charge, ξ potential is measured by electrophoretic mobility, using a zeta Malver Plus device.

When a solid such as lime is immersed in an aqueous medium, a charge develops on the surface by dissociation of functional groups from the surface or by adsorption of ions from solution. The surface charge on the lime together with the countering constitutes the electrical double layer. In the study of charged systems, three interfacial potentials are of interest, i.e., the surface, Stern-layer, and ξ potentials. The electrokinetic or ξ potential is the potential at the shear plane, where slip must occur when the solid moves relative to the liquid. The behavior of a solid particle in a liquid under these conditions is governed by charge density at the shear plane. The measurement of electrokinetic potentials is relatively easy and this is often the only direct electrical measurement that can be made. Although interpretation of the results is not straightforward, often the useful assumption is made that the slipping and Stern planes coincide. Since the ξ potential can be manipulated through adsorption of inorganic or organic ions at the Stern plane, the study of the electrokinetic behavior of the solid is of practical importance in flotation, dispersion, flocculation and therefore of the cohesion of lime particles [32].

The ξ potentials of lime particles were calculated (using the Smoluchowski model, see [33] by

$$\xi_{EP} = \frac{V\mu}{\varepsilon E_x}, \quad (2)$$

where ξ_{EP} is the electrophoretic ξ (mV), V the electrophoretic velocity (Cm/s), μ and ε the viscosity (Cp) and permittivity of the aqueous medium in standard conditions, respectively, and E_x is the axial electric field. The Smoluchowski equation is a simplified approach in which the electrostatic driving force is opposed by the frictional force; other effects are neglected. The equation is valid for solid particles with large dimensionless inverse Debye length [34]. This equation gives favourable results only for large colloidal particles and high ionic strengths, when ξ is not high. For ξ values with a practical meaning (<120 mV), the error is negligible when κa > 100, where a is particle radius and the Debye parameter κ is defined as

$$\kappa = \sqrt{\frac{F^2\sum_i C_i Z_i^2}{\varepsilon RT}}, \quad (3)$$

here, F is the Faraday constant, C_i is concentration of the i-th ion (in mol/m^3), Z is the valency of this ion, ε represents the dielectric permittivity, R is the gas constant, and T is absolute temperature.

5. Results and discussion

5.1. Chemical-mineralogical-microtextural characterization of the stone and quicklime samples and size distribution of portlandite particles

The chemical composition of major elements of the stone quarry samples and oxides obtained from the traditional kiln are shown in Table 4. It notes for the quicklime (TL, IL and PL) an increase in CaO and MgO content and reduction in content from loss on ignition LI, as expected for oxides. The PL quicklime shows the highest CaO product of analytical purity. On the other hand, the chemical composition of trace elements of the limestone and quicklime samples obtained from the traditional kiln shows in Table 5. In quarry samples; it observed Ba, Cl, and Sr contents, not present in samples of quicklime (*TL*). This can be explained by their release during the calcination of calcite.

As seen in Table 6, the mineralogical composition of the limestone used for lime production: Q1, Q2, Q3; was very similar, with calcite contents around 100%. Their biggest differences were in textural type. The Q1 lithotype corresponds to oosparite [35] with a predominance of micritic intraclasts of ooliths and foraminifera with abundant crinoids plates and sparitic cement (Fig. 3a). The Q2 Lithotype corresponds to oomicrites [35] constituted by oolites and crinoids plates with little sparitic cement and a more porous character (Fig. 3b). Finally, Q3 lithotype corresponds to a very compact micritic limestone also composed by carbonates of a micritic nature and little sparitic cement (Fig. 3c). Based on the petrographic microscope observations it conclude that the Q2 and Q3 lithotype correspond to micritic limestones, with the Q3 lithotype the most compact and homogeneous and having a lower content of macropores. The Q1 lithotype is also composed of limestone intraclasts of micritic nature, with a porosity intermediate to Q2 and Q3, but a greater content of sparitic cement and therefore more crystalline.

The microtextural observations of limestones by FESEM-se confirm the predominance of the micritic matrix in most types (calcite crystals of size <5 μm) as indicated above Fig. 4. In some cases, the presence of large carbonate crystals corresponded to crinoid plates (see Fig. 5b) and, in other cases, to recrystallized calcite in pores (see Fig. 5a), more abundant in Q1 lithotype.

From the data it concludes that these stone materials in the three lithotype are suitable for producing lime, owing to both their purity (100% calcite) and texture (dense and compact limestone). They are well suited to generate plastic limes according to Ancient Manuals Construction, for example [36]. Moreover, they correspond to low-porosity limestone, which slows the hydration after its calcination [8].

The mineralogical composition of calcium oxides obtained from these varieties of rocks is also similar, according to the two types of kilns (*TL* and *IL*). No uncooked were detected, so the calcination process was complete in both cases. Small amounts of portlandite detected in *TL*, were attributable to longer storage of CaO, which is typical of traditional lime kilns. The nanometric observation by FESEM-se (see Figs. 6, 7 and 8) of various types of CaO indicated some degree of textural similarity to the original limestones. In the case of traditional quicklime (*TL*) morphology, CaO crystals resembled the micritic calcite, indicating use of the Q2 and Q3 lithotypes. In contrast with industrial lime manufacturing, the microtexture of CaO crystals resemble more the Q1 lithotype, extracted from another area of the *Moron de la Frontera region*, specifically, *Cazalla de la Sierra* in the province of Seville similar to Q1 lithotype.

Given that the transformation of the calcite to CaO is of pseudomorphic and topotactic type [18], $CaCO_3$ microtexture controls the

Table 4
Chemical composition of major elements, expressed in wt% of oxides, for stone and quicklime materials. Loss on Ignition (LOI).

Samples	SiO2	Al2O3	Fe2O3	MnO	MgO	CaO	Na2O	K2O	P2O5	LOI
Q1	0.11	0.03	0.02	0.01	0.20	55.02	0.03	0.02	0.01	43.52
Q2	0.11	0.03	0.02	0.01	0.20	55.02	0.03	0.02	0.47	42.48
Q3	0.36	0.09	0.07	0.01	0.44	55.92	0.01	0.01	0.03	43.5
TL	0.16	–	0.04	–	0.36	75.35	0.02	0.01	0.04	9.44
IL	0.37	0.09	0.09	0.01	0.51	78.94	0.03	0.04	0.05	4.42
PL	0.97	0.27	0.26	0.01	0.58	80.61	0.02	0.02	0.02	1.35

Table 5
Chemical composition of trace elements, expressed in ppm, for samples: Q1, Q2 and *TL*.

Samples	Ba	Cl	Cr	Ga	Hf	La	Mo	Nd	Ni	Rb	Sc	Sm	Sr	Th	Tl	V	U	W	Y	Yb	Zn
Q1	51.2	50.5	1.7	8.6	4.5	18.1	1.9	10.5	0.0	2.4	20.8	2.9	78.7	4.2	0.9	6.6	0.5	5.6	11.3	1.8	51.9
Q2	33.3	27.0	0.0	9.0	3.3	17.5	1.7	11.1	8.5	0.3	16.3	2.4	55.4	2.9	0.7	2.9	0.0	1.3	10.9	1.8	52.1
TL	–	–	–	1.2	–	–	–	–	–	–	–	–	–	–	0.1	–	–	–	1.6	0.5	8.4

Table 6
Mineralogical composition of samples, expressed in wt%, for stone and quicklime materials.

Samples	CaO	Porltandite	Calcite
Q1	0	0	100
Q2	0	0	100
Q2	0	0	100
TL (1)	86	13	0
TL (2)	94	5	0
TL (3)	72	28	0
IL	95	5	0

morphology of CaO crystals in the two types of kilns. The major differences were in the textural homogeneity observed in type *TL* (see Fig. 6) and in the sample of analytical purity *PL* (see Fig. 8). In the latter case, the particles had spherical morphologies, attributable to a greater degree of sintering. Regarding CaO from industry kiln (see Fig. 7), very likely owing to microtextural heterogeneity of rock, the burning process was not uniform. It observed areas where the initial morphology of the calcite crystals appeared virtually intact, in other areas; roundness at the edges of the crystals was very visible, developing toward more porous crystals (pores generated by the release of CO_2). Ultimately, in areas where the transformation was complete, it observed morphologies similar to *TL* types. These observations show that the optimum burning conditions of the stone are specific to each lithotype, and that the thermal decomposition of calcite depends intrinsic factors of stone (micro-textual aspects), and process technology as heating speed, time and pressure of CO_2 [10].

After laboratory slaking of the various CaO type, the portlandite had the nanometer appearance shown in Figs. 9 and 10. This appearance was similar *TL*, *IL* and *PL*, in agreement with [37] who considered the transformation of CaO to $Ca(OH)_2$, also of pseudomorphic and topotactic type. However the determination of the PSD in the various suspensions portlandite obtained in the laboratory (SPL) revealed notable differences (see Fig. 11). The range of portlandite PSD in various lime suspensions was wide, 0.2–300 μm (most within 2–100 μm). Detailed observation of the various curves indicates the greater proportion of smaller particles (0.5–2 and 2–20 μm) in type SPL_{TL} (3), followed by SPL_{TL} (2), both from traditional production. The SPL_{IL} and SPL_{PL} types had smaller proportions in the aforementioned ranges, along with particle sizes between 60 and 120 μm, not present in the previously mentioned varieties. SPL_{TL} (1) (subjected to higher temperature) had grain sizes in a wider range and a distribution similar to SPL_{PL}; however, larger particles were absent and/or in smaller proportions (60–120 μm), a size range not observed or less frequent in traditional limes. Nonetheless, we note the size distribution of variety SPL_{IL} with a predominance of particles in the 2–20 μm range, similar to SPL_{TL} (3) and SPL_{TL} (2) but with greater contents of particles >50 μm.

The data (see Fig. 11) suggest that temperatures above 1000 °C, regardless of the industrial or traditional process, causes a reduction of smaller particles (in the 2–20 μm range), for example, SPL_{TL} (1) and SPL_{PL}. However, prolonged and controlled burning as in the traditional process reduces the possibility that portlandite crystals of size above 50 μm form, or reduces their proportion as in the cases of types SPL_{TL} (3), SPL_{TL} (2) and SPL_{TL} (1). This increases the content of particles of size 2–20 μm. Optimum calcination temperatures and manufacture in traditional Kilns increase the content of particles in size ranges 0.2–2 and 2–30 μm. These analyses were performed in a few weeks of slaking in the laboratory.

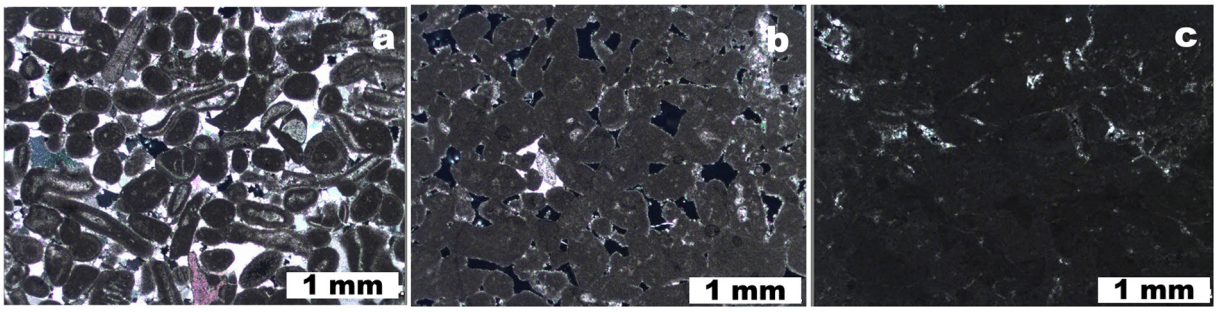

Fig. 3. Photomicrographs (plain polars) of three types of rocks used for the production of quicklime: a) Q1. b) Q2. c) Q3.

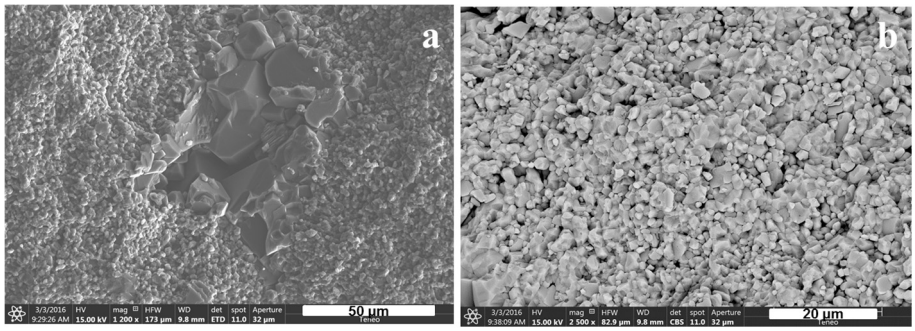

Fig. 4. FESEM-se images of limestones. a) Q2 type. b) Q3 type.

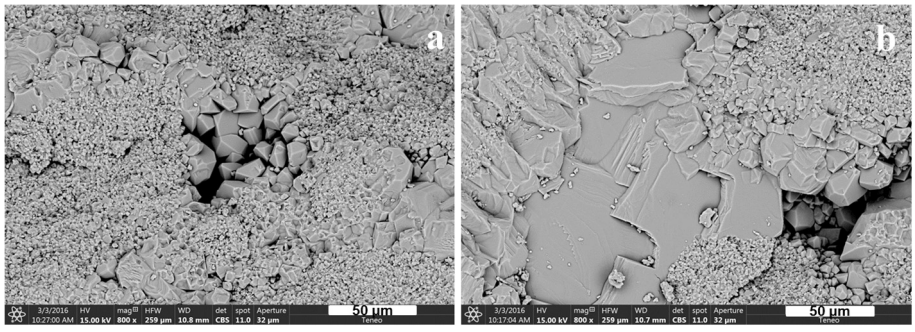

Fig. 5. FESEM-se images of Q1 type limestone. a) Crinoids plates. b) Recrystallized calcite in pores.

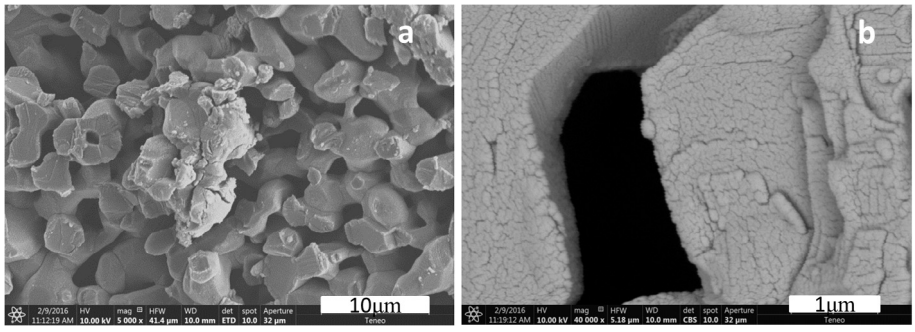

Fig. 6. FESEM-se images of TL quicklime (a and b).

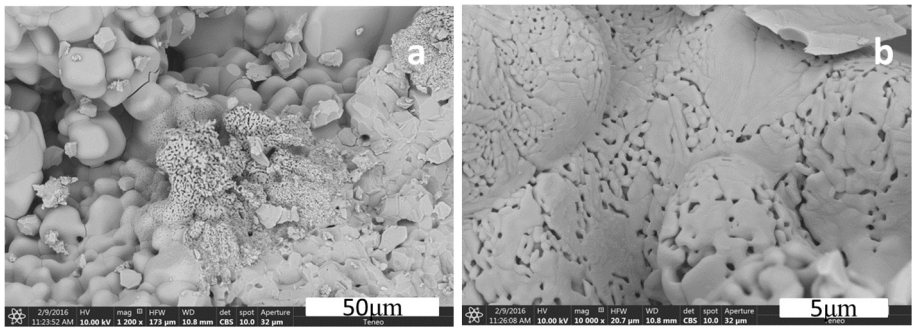

Fig. 7. FESEM-se images of IL quicklime (a and b).

5.2. Surface free energy components of lime and stone

Table 7 shows surface free energy components of different quarry stones used to obtain the various types limes. From the γ^{LW} component of the samples, we observed that Q3 lithotype had the largest value of γ^{LW} (48 mJ/m^2), whereas the other lithotypes (Q1 and Q2) had values ~43 mJ/m^2. This is likely because Q3 lithotype had a more ordered structure of water molecules at

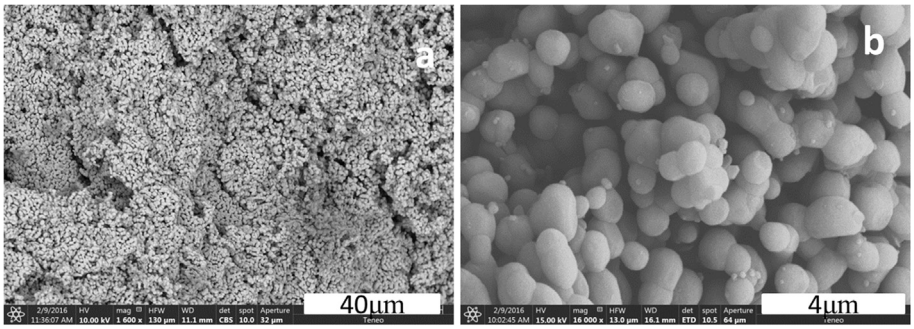

Fig. 8. FESEM-se images of PL quicklime (a and b).

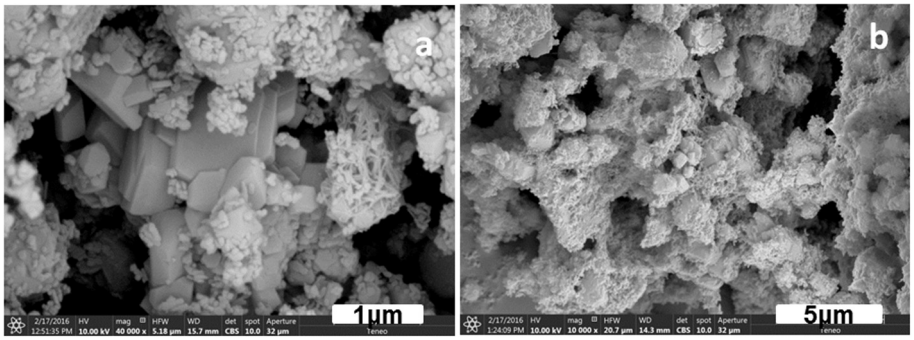

Fig. 9. FESEM-se image of slaking lime: a) SPL_{TL}. b) SPL_{IL}.

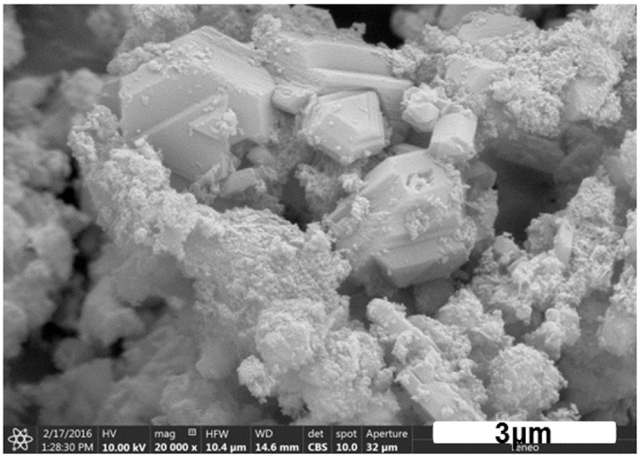

Fig. 10. FESEM-se image of SPL_{PL} slaking lime.

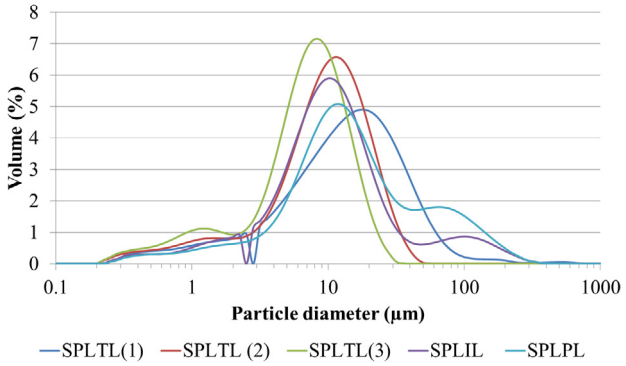

Fig. 11. Grain-size distribution of slaking lime: SPL_{TL}, SPL_{IL}, and SPL_{PL}, expressed as volume percentage.

the solid/liquid interface, so it required longer calcination. Table 7 also lists the polar components γ^+ and γ^-. This shows that the quarry stones can be considered electron-donor in nature ($\gamma^+ \approx 0$, $\gamma^- > 0$). Unlike γ^+, the electron-donor component γ^- is very sensitive to the surface composition of the rocks. However, γ^+ was not different from zero within the experimental error; i.e., all the inorganic materials in general [38] and SiO_2 [32] in particular are essentially monopolar substances in the sense of Van Oss.

Analysis of the γ^- component indicated a hydrophobic character for Q3 and Q1 lithotypes ($\gamma^- < 28.2$ mJ/m^2) and a hydrophilic character for Q2 lithotype (see Fig. 3b) with greater porosity. The lower porosity of both Q1 and Q3 lithotypes are indicated by Fig. 3a and c. Furthermore, there was in the limestones samples a tendency of increased values of γ^- and γ^{Total} for Q2 and Q3 lithotypes, the most micritic observed. The results indicate that the most crystalline limestones with larger crystal size require longer calcination. The rocks with smaller crystal sizes had greater surface area and therefore burning would be more rapid. It is also interesting to know the effect of other factors such as the purity of the stone, of interest for future works.

Table 8 shows values of γ^+ and γ^- of the two lime types (TL and IL) from the three lithotypes of rocks. The results show that the calcination process substantially changes the surface free energy components, as expected from the chemical change experienced by the material after its transformation from carbonate to oxide. It emphasize that the quicklime (CaO) is monopolar (electron donor) and has a hydrophilic nature ($\gamma^- > 28.2$ mJ/m^2). Considering the electron donor component, the data shows that the most hydrophilic was *PL* quicklime, followed by *TL* and *IL*.

Table 9 shows values of surface free energy of quicklime obtained in the traditional kiln, according to various calcination temperatures reached within its interior. γ^{Total} values decreased with increasing calcination temperature. Therefore, oxide obtained

Table 7
Surface free energy components of quarry limestone (mJ/m^2).

Liquid	γ^{TOTAL}	γ^{LW}	γ^+	γ^-
Q1	50	42	0.6	24
Q2	54	44	0.5	50
Q3	57	48	1.8	11

Table 8
Surface free energy components of quicklimes (mJ/m^2): Traditional quicklime (TL), industrial quicklime (IL) and analytical purity quicklime (PL).

Liquid	γ^{TOTAL}	γ^{LW}	γ^+	γ^-
TL (2)	52.17	48.6	0.05	57
IL	49.57	39.1	0.76	35.9
PL	60.03	47.78	0.60	62.36

Table 9
Surface free energy components (mJ/m^2) of quicklime (Ca0) of traditional manufacture, for three calcinations temperatures: *TL* (1): 1100 °C, *TL* (2): 900 °C, and *TL* (3): 850 °C.

Liquid	γ^{TOTAL}	γ^{LW}	γ^+	γ^-
TL(1) 1100 °C	47.3	38.1	0.68	31.3
TL(2) 900 °C	52.17	48.6	0.05	57
TL(3) 850 °C	55.9	48.1	0.37	45.6

Table 10
Surface free energy components (mJ/m^2) of slaking limes, Ca ($0H_2$), for different types of quicklime: TL (traditional manufacture), IL (industrial manufacture) and PL Panréac with analytical purity, slaked in the laboratory.

Liquid	γ^{TOTAL}	γ^{LW}	γ^+	γ^-
SPL_{TL} (1)	46.33	44.22	0.061	18.07
SPL_{TL} (2)	58.63	47.48	0.56	55.03
SPL_{TL} (3)	57.62	46.50	0.43	71.45
SPL_{IL}	49.62	48.07	0.009	49.62
SPL_{PL}	48.87	48.6	0.00035	50.2

Table 11
ξ potential (mV) for different limestones: Q1, Q2, Q3 and quicklimes (TL (1), TL (2) and TL (3), IL and PL.

Samples	ClNa 10^{-3}
Q1	−17.05
Q2	−16.35
Q3	−17.35
TL (1)	32.1
TL (2)	34.7
TL (3)	34.7
IL	4.63
PL	19.16

at higher temperature has less surface free energy. From the donor electron component analysis, it conclude that the CaO subjected to higher temperature (1100 °C) is less hydrophilic and thus its hydration capacity is less or needs more time to complete hydration. This suggests that the burning time of the stone as well as the temperatures reached have an important role [5].

Table 10 shows surface free energy components values of lime putty (SPL) in the laboratory from the various quicklimes (*TL*, *IL* and *PL*). The results shows that hydration of quicklime modifies the surface free energy components, but not in the same way for all samples. For example, for SPL_{TL}, those components were practically unchanged. In contrast, industrial production lime is hydrophilized substantially, with γ^- changing from 35.9 to 49.62 mJ/m^2. There was a similar result for the lime of analytical purity. From these data it can say that the sample of putty lime from traditional manufacturing had increased hydrophilicity and therefore a greater capacity of water retention, consonant with [3,39]. This explains the greater volume acquired by the hydrated lime from traditional production, which can be as much as three times the initial volume [7].

For the traditional lime, Table 10 reveals the effect of the rock calcination temperature on the process outcome, i.e., the formation of hydroxide. Regarding the surface energy components, for SPL_{TL} (1), γ^- values for *TL* (1) passed from 31.3 to 18.07 mJ/m^2 during hydration, with both oxide and hydroxide samples having greater hydrophobicity (thereby requiring longer hydration). From the data in Table 11, it concludes that the higher the calcination temperature the hydroxides reached, the greater their hydrophobicity.

The study of the surface free energy components of lime and limestone indicates the effects of temperature and time of calcination of the stone. These data show the importance of maximum temperature, so an excessive temperature increase and short period of calcination appear to be factors unfavorable to the quality of lime.

5.3. ξ Potential of samples

Table 11 shows data of ξ potential of different sample analyzed ionic strength constant of 10^{-3} of NaCl. Stone quarry samples from *Gilena* and *Moron de la Frontera* (both near Seville) showed appreciable difference in obtained values. ξ potential was negative in all cases with values around −17 mV, similar to data for calcite obtained by others authors [40]. Using the Gilena stone, it performed calcination to calcium oxide to obtain traditional lime.

Table 11 also shows the ξ potential of various types of CaO. The ξ potential of CaO obtained by the traditional process (*TL*) gave values passing from 32.1 to 34.7 mV. These values are much larger than that of the industrial process (*IL*) (4.63 mV); the *PL* quicklime value was 19.16 mV. It therefore concluded that traditional production oxides have a greater charge than those from industrial production (see Fig. 12).

The results also show that the oxides from traditional kilns have similar values of ξ potential, regardless of their position in the kiln. Therefore, the temperature factor in the studied margins (1100–850 °C) does not appear to be a determinant in the generation of charge.

It also determined the ξ potential of the slaked lime in the laboratory from the various types of quicklime (see Table 12). The data indicate that ξ potential decreased compared to their oxide of origin, losing charge during hydration. An analysis of aging putty lime (see Table 12) shows that this loss of charge over time is prolonged with time of contact with water. This has been demonstrated by leaving the slaked lime in a sealed container for six months. This may be in line with the work of [25], which indicated that lime has better properties just after slaking.

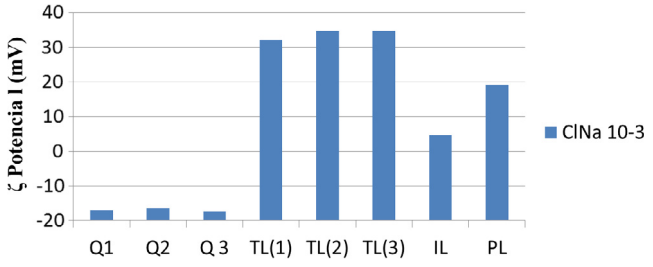

Fig. 12. ξ potential (mV) of quarry stones and quicklime (*TL*, *IL* and *PL*).

Table 12
ξ potential (mV) of different samples of slaked limes in the laboratory.

Samples	ξ Potencial (Time, 0)	ξ Potencial (Time, 6 month)	
SPL_{TL} (1)	ClNa 10^{-3}	24.6	18.6
SPL_{TL} (2)	ClNa 10^{-3}	25.35	20.05
SPL_{TL} (3)	ClNa 10^{-3}	24.7	29.2
SPL_{IL}	ClNa 10^{-3}	3.36	1.6
SPL_{PL}	ClNa 10^{-3}	11.93	1.7

Table 13
ξ potential (mV) of commercial traditional putty lime SPL_{TI} at different times (6 months–10 years).

Samples	ξ Potencial (Time)	
SPL_{Tc} (6 months)	ClNa 10^{-3}	20.35 mV
SPL_{Tc} (10 years)	ClNa 10^{-3}	26.1 mV

The results also show that hydrated lime from SPL_{TL} production had a greater charge than that from SPL_{IL}, with 25 mV versus 3.35 mV. Notably, ξ potential values of SPL_{IL} and SPL_{PL} lime were very small, which explains the presence of aggregates of size above 50 μm seen in Fig. 11. Moreover, slaking lime permanence in water for six months produces shielding of charge to near disappearance.

The temperature used in the manufacture of traditional quicklime also impacts on the hydroxide charge and evolution during the aging putty lime process. The results show that temperature does not affect the value of ξ potential of the material at t = 0, however, for an aging period of six months, the portlandite from quicklime formed at high temperatures (1100 °C) in the traditional kiln loses some charge. In contrast, the behavior at 850 °C showed an increase of charge up to 29.2 mV.

The above demonstrates the importance of maintaining an optimal, constant temperature in the kiln. Further, it explains the structure of traditional kilns, constructed with the proper burning stone and filled with fragments of varying size (from large to small as a function of distance from the center or focus of heat) and covered by a layer of clay (which is replenished while the kiln is operating) to prevent the escape of heat [29].

These results indicate the importance of proper burning of the stone, because this favors the increase of CaO charge and, after his slaking generates portlandite particles of greater electrophoretic mobility. This results in a larger proportion of small particles.

To complement the present investigation it made a comparative study with traditional lime (SPL_{Tc}), slaking by fusion with mechanical agitation in large amounts of oxide over 30 days with different periods of aging lime putty (6 months and 10 years). ξ Potential data are shown in Table 13. The results indicate that lime slaked on shelves by melting retains greater charge and, after 10 year's aging, the lime retains values greater than that recently slaked in the laboratory. This confirms that recently slaked lime has optimal conditions of plasticity that are maintained or improved with aging [41]. The data of ξ potential confirm the superior plasticity properties of traditional lime and that this quality is maintained over time.

6. Conclusions

The optimum burning conditions of the limestone are specific to each lithotype, and that the thermal decomposition of calcite depends intrinsic factors of stone and process technology as heating speed, time and pressure of CO_2. The results indicate that the most crystalline limestones with larger crystal size and lower porosity require longer calcination. The rocks with smaller crystal sizes had greater surface area and therefore burning would be more rapid.

The calcination process of limestone modifies the surface free energy components of the rock. The resulting, CaO has a hydrophilic nature but with a character dependent on the type of kiln. Specifically, quicklime is more hydrophilic when produced in a traditional kiln, and when the temperature is ~900–850 °C. Moreover, less porous limestone requires higher temperature and longer firing time, based on its γ^{Total} values.

The study of the surface free energy components of lime and limestone indicates the effects of the density, porosity and crystal size of the rock via the variation of those components, as well as the importance of temperature and time of calcination of the stone. The CaO subjected to higher temperature (1100 °C) is less hydrophilic and thus its hydration capacity is less or needs more time to complete hydration. These data indicate the importance of maximum temperature, so an excessive temperature increase and short period of calcination appear to be factors unfavorable to the quality of lime.

The limestone microtexture controls the morphology of CaO crystals in the two types of kilns. The major differences were due to textural homogeneity, but the transformation of CaO to Ca $(OH)_2$ in the traditional process reduces the possibility of formation of portlandite crystals >50 μm.

Samples of slaking lime from traditional manufacturing had greater hydrophilicity. This indicates that lime so produced has a greater water retention capacity. The calcination temperature also affects the charge acquired by portlandite [$Ca(OH)_2$]. Therefore, for firing temperatures ~900–850 °C, the calcium hydroxide not only does not lose charge but it increases.

Values of ξ potential of quicklime (CaO) obtained via the traditional process were much larger than those from the industrial process (less charge). The analytical purity sample had greater charge than industrial quicklime but less than the traditional lime. Therefore, the traditional process generates products with greater electric charge and hence with more plasticity.

The findings highlight the importance of firing time and improvement in the calcination process of the stone, for increasing the charge of the resulting quicklime (CaO) and promoting greater electrophoretic mobility of portlandite particles.

This study shows that traditional lime behaves as hydrophilic colloids (lyophilic), corresponding to colloidal systems that have strong affinity for solvent; its viscosity is typically high and usually reversible.

Acknowledgements

We gratefully acknowledge the support of the institutions involved. This work was partially funded by two projects: the MEDSUV project from the European Union Seventh Framework Programme (FP7) under Grant No. 308665, and the Spanish Government (Project CGL2011-29499-C02-01) and Project – *Standardization of the use of lime for its application in conservation of Cultural Heritage*-. Andalusian Historical Heritage Institute. Spain (IAPH).

References

[1] J. Ashurst, F. Dimes, The cleaning and treatment of limestone by the lime method, Conserv. Build. Decorative Stone 2 (1990) 169–184.
[2] E.F. Hansen, C. Van Rodríguez-Navarro, K. Balen, Lime putties and mortars: insights into fundamental properties, Stud. Conserv. 53 (2008) 9–23.
[3] R.S. Boynton, Chemistry and Technology of Lime and Limestone, Wiley, New York, 1980.
[4] J.A. Murray, Summary of Fundamental Research on Lime and Application of Results to Commercial Problems, Report of National lime Association, Washington, DC, 1956.
[5] J.L. Eqdes, P.A. Sandberg, Characterization of the properties of comercial lime by suface area measurment and scanning electro microscopy. The reactions parameters of lime, Am. Soc. Test. Mater. (1970) 3–23.

[6] S. Pavia, S. Carol, An investigation of roman mortar technology through the petrographic analysis of archaeological material, Constr. Build. Mater. 22 (2008) 1807–1811.
[7] F. Alou, V. Fulan, Materiaux de construcción, Chapitre II. Liants mineraux, Ecole Polytecnhnique Fedreale de Lausance, Lausanne, 1989.
[8] A. Moropoulou, A. Bakolas, E. Aggelakopoulou, The effects of limestone characteristics and calcination temperature to the reactivity of the quicklime, Cem. Concr. Res. 31 (2001) 633–639.
[9] D.C. Hughes, K. Callebaut, In situ visual analysis and practical sampling of historical mortars, Mater. Stuct. 35 (2002) 70–75.
[10] S. Maitra, N. Bandyopadhyay, S. Das, A.J. Pal, J. Pramanik, Non-isothermal decomposition kinetics of alkaline earth metal carbonates, J. Am. Ceram. Soc. 90 (2007) 1299–1303.
[11] E. Ruiz Agudo, C. Rodríguez Navarro, Microstructure and rheology of lime putty, Langmuir 26 (2010) 3868–3877.
[12] J.R. Rosell, Aportaciones al conocimiento del comportamiento deformacional de pastas de cal. Tamaño y formas de las partículas y su viscosidad, Tesis Doctoral, Universidad Politécnica de Cataluña (2010), 251, 2013.
[13] R. Rodríguez-Clemente, J. Gómez-Morales, A. López-Macipe, J. Garcia-Carmona,M. Ocaña, C.J. Serna, Solid particles formation from solutions, an intellectual and industrial meeting point and challenge, Contrib. Sci. 1. 1, Institut d'Estudis Catalans, Barcelona, 1999, pp. 63–77.
[14] O. Rodríguez Cazalla, C. Navarro, E. Sebastián, G. de la Cultrone, M.J. Torre, Aging o lime putty: effects on tradicional lime mortar carbonation, J. Am. Ceram. Soc. 38 (5) (2000) 1070–1076.
[15] K. Elert, C. Rodríguez-Navarro, E. Sebastián, E. Hansen, O. Cazalla, Lime mortars for the conservation of historic buildings, Stud. Conserv. 47 (2002) 62–75.
[16] C. Rodríguez Navarro, E. Ruiz Agudo, M. Ortega Huertas, E. Hansen, Nanostructure and irreversible colloidal behavior of $Ca(OH)_2$: implications in cultural heritage conservation, Langmuir 21 (2005) 10948–10957.
[17] G. Mascolo, M.C. Mascolo, A. Vitale, Microstructure evolution of lime putty upon againg, J. Cryt. Growth 312 (116–17) (2010) 2363–2368.
[18] C. Rodríguez Navarro, E. Ruiz Agudo, A. Luque, C. Rodríguez Navarro, M. Ortega Huertas, Thermal decomposition of calcite: mechanisms of formation and textural evolution of CaO nanocrystals, Am. Mineral. 94 (2009) 578–593.
[19] C.J. Van Oss, M.K. Chaudhury, R.J. Good, Chem. Rev. 88 (1988) 927.
[20] C.J. Van Oss, Interfacial Forces in Aqueous Media, Marcel Dekker, New York, 1994.
[21] A. Arizzi, R. Hendrickx, G. Van Cultrone, K. Balen, Differences in the rheological properties of calcitic and dolomitic lime slurries: influence of particle characteristics and practical implications in lime-based mortar manufacturing, Materiales de Construcción 62 (306) (2012) 231–250.
[22] Y. Sébaïbi, R.M. Dheilly, M. Quéneudec, A stady the viscosity of lime-cement pasta. Influence of the physic-chemical carateristics of lime, Const. Build. Mater. (2004) 635–660.
[23] S. Dash, M. Kamruddin, P.K. Ajikumar, A.K. Tyagi, B. Raj, Nanocrystalline and metastable phase formation in vacuum thermal decomposition of calcium carbonate, Thermochim. Acta 363 (2000) 129–135.
[24] D. Beruto, A.W. Searcy, M.G. Kim, Microstructure, kinetic, structure, thermodynamic analysis for calcite decomposition: free-surface and powder bed experiments, Thermochim. Acta 424 (2004) 99–109.
[25] E. Ruiz Agudo, C. Rodriguez Navarro, Rheology and microstructure of lime putty: implications in the design of mortars for conservation purposes, IX congreso Internacional (CICOP) de Rehabilitación del Patrimonio Arquitectónico y Edificación, 2008, pp. 152–158.
[26] A. Luque, E. Sebastián Pardo, E. Ontiveros, J. Espinosa, Morteros de cal: una propuesta para la intervención en la iglesia San Miguel de Jerez.Actas de la III Bienal de Restauración Monumental, Sobre la des-Restauración, ISBN: 978-84-8266-820-8. 2006, IS. Consejería de Cultura. Instituto Andaluz del Patrimonio Histórico y Academia del Partal, 2008, pp. 259–264.
[27] R. Rodríguez García, A. Gonzalez Serrano, J. Ganivell García de Paredes, A. Romero Jirón, La Cal de Morón en la arquitectura Tradicional Andaluza, En: Patrimonio Cultural de España, vol. 8, 2014, pp. 213–225.
[28] G. Carrera, M. Olivi, La al investigación, patrimonio y restauración, Fical (2014) 149–166.
[29] G. Carrera Díaz, Cal de Morón, Ser calero en Morón de la Frontera (Sevilla, España), Ejemplo de Buenas Prácticas Salavaguarda del Patrimonio Inmaterial de la Humanidad, En Cal viva. (Ed.) Asociación Cultural de Hornos de la Cal de Morón, ISBM: 978-84-606-5983-9, 2015, pp. 111.
[30] J. Cruz-Sanjulian, Estudio geológico del sector Cañete la Real. Teba-Osuna (Cordilleras Béticas, región occidental), Tesis doctoral Universidad de Granada, n° 71, Secretariado de Pub, Universidad de Granada XII, 1974, pp. 431.
[31] P. Ortiz, E. Mayoral, M.A. Guerrero, E. Galán, Caracterización petrográfica y geoquímica de las calizas de la Sierra de Estepa (Sevilla) y evaluación de la calidad técnica como material de construcción, Estudios Geol. 51 (1995) 213–222.
[32] A. Ontiveros-Ortega, F. Vidal, E. Giménez, J.M. Ibañez, Effect of heavy metals on the surface free energy and zeta potential of volcanic glass: implication on the adhesion and growth of microorganism, J. Mater. Sci. 49 (2014) 3550–3559.
[33] H. Ohshima, T.H. Healy, L.R. White, Accurate analytic expressions for the surface charge density/surface potential relationship and double-layer potential distribution for a spherical colloidal particle, J. Colloid Interface Sci. 90 (1982) 17–26.
[34] M. Wang, A. Revil, Electrochemical charge of silica surfaces at high ionic strength in narrow channels, J. Colloid Interface Sci. 343 (2010) 381–386.
[35] R. Folk, Petrology of Sedimentary Rocks, (Ed.) Hemphill's, Austin, 1968, pp. 170.
[36] C.A. Jombert, Architecture moderno u lárt de bien bâtir pour toutes sortes de personnes tant pour les maisons des particuliers que pour les palais, Contenabt cinq traites Genova. Tomo I y II, 1728, 1973.
[37] K. Kudlacz, C. Rodríguez Navarro, The mechanism of vapor phase hydration of calcium oxide: implications for CO2 capture, Environ. Sci. Technol. 21 (2014) 12411–12418.
[38] I. Plaza, A. Ontiveros-Ortega, J. Calero, V. Aranda, The Implication of ξ potential and surface free energy in the description of agricultural soil quality: effect of different cations and humic acids on degraded soils, Soil Tillage Res. 146 (2014) 148–158.
[39] J. Arhurst, N. Arhurst, Mortars, platers and redenrs, Southampto, Gower Technical Press edition de English Heritage Technical Handbook, Practical Building Conservation, vol. 3, 1989.
[40] J. Duran, A. Ontiveros, A.V. Delgado, F. Gonzalez-Caballaro, Kinetics and interfacial interactions in the adhesion of colloidal calcium carbonate to glass in a packed-bed, Appl. Surf. Sci. 134 (1998) 125–138.
[41] C. Atzeni, A. Farsi, D. Floris, P. Meloni, Effect of Aging on Rheological. Properties of Lime Putty, J. Am. Ceram. Soc. 87 (2004) 1764–1766.